

Front propagation in three-dimensional corrugated reaction-diffusion media

S. Martens,^{1,*} J. Löber,¹ and H. Engel¹

¹*Institut für Theoretische Physik, Hardenbergstraße 36, EW 7-1,
Technische Universität Berlin, 10623 Berlin, Germany*

Propagation of traveling fronts in three-dimensional reaction-diffusion media with spatially modulated cross-section is studied using the Schlögl model as a representative example. Applying appropriate perturbation techniques leads first to a reduction of dimensionality in which the spatially dependent Neumann boundary condition translate into a boundary-induced advection term and, secondly, to an equation of motion for the traveling wave position in weakly corrugated confinements. Comparisons with numerical simulations demonstrate that our analytical results properly predicts the nonlinear dependence of the propagation velocity on ratio of the spatial period of the confinement to the intrinsic width of the front; including the peculiarity of propagation failure. Based on the eikonal equation, we obtain an analytical estimate for the finite interval of propagation failure. Lastly, we demonstrate that the front velocity is determined by the suppressed diffusivity of the reactants if the intrinsic width of the front is much larger than the spatial variation of the medium.

PACS numbers: 05.40.Jc, 05.45.-a, 82.33.-z, 82.40.Qt, 89.75.Kd

I. INTRODUCTION

Propagating fronts are one of the simplest examples of traveling wave activity in dissipative spatially extended systems. Like excitation pulses, periodic pulse trains, spiral and scroll waves, they are examples of nonlinear waves and represent fascinating self-organized spatio-temporal patterns in nonequilibrium macroscopic systems. Traveling waves have been observed in many physical [1], biological [2–4], and chemical systems [5, 6]. Prominent examples of front propagation include catalytic oxidation of carbon monoxide (CO) on platinum single crystal surfaces [7–10], arrays of coupled chemical reactors [11], and nematic liquid crystals [12].

Often, the medium that supports front propagation exhibits a complex shape and/or its size is limited like in biological cells [13], nanoporous media [14], or zeolites [15]. In such system the interaction of the reactants with the boundaries of the medium leads to non-intuitive confinement effects. For example, phase separation in porous materials results in layering, freezing, wetting and other novel phase transitions not found in the bulk system [16]. In particular, both competing processes facilitating the propagation of traveling waves, viz., the chemical autocatalysis [17] and the molecular diffusion [18–20], strongly depend on the shape of the domain. Recent studies on the fundamental problem of particle transport through micro-domains exhibiting obstacles and/or small openings showed that the shape of these confinements (periodicity, size of the connecting openings) regulates the dynamics of diffusing particles leading to transport properties which significantly differ from free Brownian motion [21–24].

Even in systems ranging from micro- to the macroscale there is a ongoing interest in studies of nonlinear wave

propagation under spatially confined conditions. Important issues investigated in this context are the dependence of front reflection on the geometry size in the catalytic CO oxidation on platinum surfaces [25], reaction fronts in Poiseuille [26] or shear flows [27], three-dimensional (3D) traveling waves in the human heart [28], to name a few. Some parts of the human heart tissue, especially at the ventricles, are thick enough to support not only spiral waves, but also 3D vortex structures, for example scroll waves and scroll rings. Therefore, detailed knowledge about the interaction of these self-organized spatio-temporal patterns with boundaries [29, 30], at most a few vortex wavelengths away, is important for the understanding of possible mechanisms responsible for atrial tachycardia.

Nowadays, well-established techniques like micro-lithography enables to design the shape of reactive domains as well as to prescribe the geometry. This provides an efficient method to study experimentally the impact of confinement on front propagation and to control and optimize, respectively, the local dynamics of catalytic reactions.

In this paper, we address the problem of traveling front propagation through a three-dimensional reaction medium with periodically modulated cross-section. Aiming at deriving an equation of motion for the front position in a corrugated media, we apply asymptotic perturbation analysis in a geometric parameter [24, 31] and projection techniques [32–34] to the problem. Our goal is to analyze how spatial variations of the cross-section of the media affect front propagation. In detail, we will discuss the dependence of the propagation velocity on the spatial period of the confinement, the size of the connecting openings, and on the kinetic parameter of the local reaction. Furthermore, we focus on boundary-induced phenomena such as propagation failure and effective diffusivity.

The paper is organized as follows: In Sec. II, we state the general problem for a n -component reaction-diffusion

* steffen.martens@tu-berlin.de

(RD) system in a 3D media with spatially modulated cross-section. In Sec. II A and II B, we present perturbation methods in order to reduce the dimensionality of the problem and to derive an equation of motion for the traveling front. Additionally, we obtain analytical expressions for the average front velocity. In Sec. III, we compare our general results with numerical simulations for the one component Schlögl model. An analytical estimate for the finite interval of propagation failure is presented in Sec. III A. In Sec. IV, we demonstrate that the front velocity is determined by the suppressed diffusivity of the reactants if the intrinsic width of the front is much larger than the spatial variation of the medium. Finally, we conclude our results in Sec. V.

II. STATEMENT OF THE PROBLEM

We consider a reaction-diffusion (RD) system for the vector of n concentration fields $\mathbf{u} = \mathbf{u}(\mathbf{r}, t) = (u^1, \dots, u^n)^T$ whose spatial and temporal evolution is modeled by a partial differential equation (PDE)

$$\partial_t \mathbf{u} = \mathbb{D} \Delta \mathbf{u} + \mathbf{R}(\mathbf{u}) \quad (1)$$

in a three-dimensional medium with position vector $\mathbf{r} = (x, y, z)^T$. Here, $\mathbb{D} = \text{diag}(D_1, \dots, D_n)$ is the diagonal matrix of constant diffusion coefficients, Δ denotes the Laplacian operator, and $\mathbf{R}(\mathbf{u})$ represents the local, non-linear reaction kinetics. The reaction medium is assumed to be uniform, isotropic, and infinitely extended in the x -direction. In the transverse directions, the medium is confined by periodically modulated walls at $y = \omega_{\pm}(x)$, with spatial period L_x and plane walls placed at $z = 0$ and $z = \Delta H$. For convenient, the height is set to unity $\Delta H = 1$. A sketch of the setup is depicted in Fig. 1. Because of the channel walls' impermeability with respect to diffusion the material flux obeys no-flux boundary conditions (b.c), reading

$$(\nabla \mathbf{u}(\mathbf{r}, t)) \cdot \mathbf{n}(\mathbf{r}) = 0, \quad \forall \mathbf{r} \in \text{channel wall}. \quad (2)$$

$\mathbf{n}(\mathbf{r})$ denotes the out-pointing normal vector at the channel walls, viz. $\mathbf{n}_z = (0, 0, \pm 1)^T$ at $z = 0, \Delta H$ and $\mathbf{n}_{\pm} = (\mp \omega'_{\pm}(x), \pm 1, 0)^T$ at $y = \omega_{\pm}(x)$ with the prime denoting the differentiation with respect to x .

Passing to dimensionless quantities, all lengths are measured in units of the widest cross-section of the channel $\Delta\Omega$, yielding $\mathbf{r} \rightarrow \Delta\Omega \bar{\mathbf{r}}$. The time is scaled in units of the intrinsic time scale on which the one of the n reactions takes place, $t \rightarrow \bar{t}/k_{\text{reac}}$, with the so-called reaction coefficient k_{reac} . Thus, the re-scaled diffusion constants read $\mathbb{D} \rightarrow \Delta\Omega^2 k_{\text{reac}} \bar{\mathbb{D}}$.

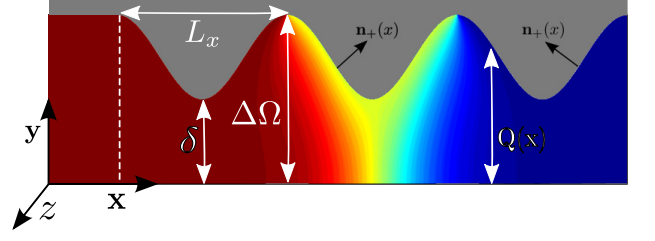


Figure 1. (Color online) Plan view on a segment of the reaction medium with spatially modulated cross-section $Q(x)$. The media is confined by sinusoidally modulated boundaries at $y = \omega_{\pm}(x)$, with spatial period L_x , and by plane walls placed at $z = 0$ and $z = \Delta H$; ΔH represents the channel height. The bottleneck size and the maximum channel width are δ and $\Delta\Omega$, respectively. The out-pointing normal vector \mathbf{n}_x at the upper transverse channel wall $\omega_+(x)$ is indicated by the arrows. The dashed line indicates the begin of the boundary corrugation in the numerical simulations. Superimpose is the concentration field $u(\mathbf{r}, t)$ of a front traveling from the left to the right.

A. Asymptotic perturbation analysis

Below, we perform asymptotic perturbation analysis in the dimensionless geometric parameter

$$\varepsilon = (1 - \delta)/\bar{L}_x \ll 1, \quad (3)$$

which characterizes the deviation of the corrugated walls ω_{\pm} from flat structures, i.e., $\varepsilon = 0$; δ denotes the ratio of the bottleneck width $\Delta\omega$ to the maximal channel width $\Delta\Omega \equiv 1$. The choice for the expansion parameter ε is motivated by previous studies on the problem of Brownian motion in corrugated channels [24, 31]. Upon re-scaling the transverse coordinate $y \rightarrow \varepsilon \bar{y}$, the profile functions become $\omega_{\pm}(\bar{x}) \rightarrow \varepsilon h_{\pm}(\bar{x})$ and the outward pointing normal vector at the perpendicular side-walls is given by $\mathbf{n}_{\pm} = (\mp \varepsilon h'_{\pm}(x), \pm 1, 0)^T$. Thus, the no-flux boundary condition Eq. (2) transforms to

$$(\nabla \mathbf{u}(\mathbf{r}, t)) \cdot \mathbf{n}(\mathbf{r}) = 0 = \mp \varepsilon^2 h'_{\pm}(\bar{x}) \partial_{\bar{x}} \bar{\mathbf{u}} \pm \partial_{\bar{y}} \bar{\mathbf{u}}, \quad (4)$$

at $\bar{y} = h_{\pm}(\bar{x})$. In the following, we shall omit the overbar in our notation.

Expanding \mathbf{u} in a series in even powers of ε , we get $\mathbf{u}(\mathbf{r}, t) = \mathbf{u}_0(\mathbf{r}, t) + \varepsilon^2 \mathbf{u}_1(\mathbf{r}, t) + \mathcal{O}(\varepsilon^4)$. Substituting this ansatz into Eq. (1) and observing the no-flux boundary conditions Eq. (4), we obtain a hierarchic set of coupled partial differential equations. To derive the leading order term, one has to solve $\mathbb{D} \partial_y^2 \mathbf{u}_0 = 0$ supplemented with the corresponding no-flux boundary conditions, namely, $0 = \pm \partial_y \mathbf{u}_0$ at $y = h_{\pm}(x)$ and $0 = \pm \partial_z \mathbf{u}_0$ at $z = 0, \Delta H$. It immediately follows that the concentration profiles $\mathbf{u}_0(\mathbf{r}, t) = \mathbf{g}(x, t)$ are flat in y and z direction. The unknown function $\mathbf{g}(x, t)$ has to be determined from the second order $\mathcal{O}(\varepsilon^2)$ balance given by

$$\partial_t \mathbf{u}_0 = \mathbb{D} (\partial_x^2 \mathbf{u}_0 + \partial_y^2 \mathbf{u}_1 + \partial_z^2 \mathbf{u}_0) + \mathbf{R}(\mathbf{u}_0). \quad (5a)$$

Integrating the latter over the local cross-section $Q(x) = \Delta H(\omega_+(x) - \omega_-(x))$ and taking the no-flux boundary conditions

$$0 = \mp h'_\pm(x) \partial_x \mathbf{u}_0 \pm \partial_y \mathbf{u}_1, \quad \forall y = h_\pm(x), \quad (5b)$$

into account, one obtains

$$\partial_t \mathbf{u}_0(x, t) = \mathbb{D} \partial_x^2 \mathbf{u}_0 + \mathbf{R}(\mathbf{u}_0) + \mathbb{D} \frac{Q'(x)}{Q(x)} \partial_x \mathbf{u}_0. \quad (6)$$

Above, we address the problem of the propagation of traveling wave (TW) solutions to RD systems through 3D channel geometries exhibiting spatially modulated cross-section $Q(x)$. Applying asymptotic analysis in a geometric parameter ε , determining the channel's cross-section changing rate, leads to an approximate description that involves a reduction of dimensionality; the propagation of traveling waves in spatially varying confinements reduces to a one-dimensional RD equation with an additional *boundary-induced advection term* Eq. (6). The advective velocity field $\mathbf{v} = Q'(x)/Q(x) \mathbf{e}_x$ is compressible, $\nabla \cdot \mathbf{v}(x) \neq 0$, reflects the periodicity of the channel modulation L_x , $\mathbf{v}(x + L_x) = \mathbf{v}(x)$, and has zero mean, i.e. $\int_0^{L_x} dx \mathbf{v}(x) = \mathbf{0}$. It has been shown [35] that stable traveling wave solutions exist in reaction-diffusion-advection systems like Eq. (6). Referring to Eq. (6), a front propagating from left to right, $\partial_x \mathbf{u}_0 < 0$, becomes decelerated where the channel expands $Q'(x) > 0$ and is accelerated if the channel contracts $Q'(x) < 0$, respectively. The derivation of Eq. (6) entails a tacit requirement, namely, the existence of a hierarchy of relaxation times [36, 37]. This hierarchy guarantees the separation of time scales and supports the approximation that the reactants diffuse much faster in transverse directions than in the propagation (x -) direction. Consequently, the leading order concentration profiles are flat in y and z direction for any spatial variation of $Q(x)$.

B. Projection method – multiple scale analysis

We are interested in the response of the TW to the boundary-induced advection term $\mathbb{D}(\mathbf{v} \cdot \nabla) \mathbf{u}_0 \propto Q'(x)$. We derive this term under the assumption that the channel's cross-section changes weakly, i.e., $\max(|Q'(x)|) \simeq \varepsilon$. Therefore, we interpret the advection term as a weak perturbation to the 1D RD system, $\partial_t \mathbf{u}_0(x, t) = \mathbb{D} \partial_x^2 \mathbf{u}_0 + \mathbf{R}(\mathbf{u}_0)$. Previous works considering the effect of parameter fluctuations [32], parameter heterogeneities [33], or weak spatio-temporal controls $\mathbf{f}(\mathbf{u}, \mathbf{r}, t)$ [34] on the front propagation demonstrate that the projection method can properly predict the dynamics of TW under weak perturbations.

Next, we sketch the basic ideas behind the projection method: We presume that the RD system Eq. (6) exhibit a TW solution \mathbf{U}_c in channels with constant cross-section $Q(x) = \text{const}$, i.e., $\mathbf{v}(x) = \mathbf{0}$. These solutions are stationary in frame of reference $\xi = x - c_0 t$ co-moving with the

velocity c_0

$$0 = \mathbb{D} \partial_\xi^2 \mathbf{U}_c + c_0 \partial_\xi \mathbf{U}_c + \mathbf{R}(\mathbf{U}_c). \quad (7)$$

The eigenvalues of the linear operator

$$\mathcal{L} = \mathbb{D} \partial_\xi^2 + c_0 \partial_\xi + \mathcal{D}\mathbf{R}(\mathbf{U}_c). \quad (8)$$

determine the stability of the TW, where $\mathcal{D}\mathbf{R}(\mathbf{U}_c)$ denotes the Jacobian matrix of \mathbf{R} evaluated at the TW. We assume $\mathbf{U}_c(\xi)$ to be stable. Therefore the eigenvalue of \mathcal{L} with the largest real part is $\lambda_0 = 0$ and the Goldstone mode $\mathbf{W}(\xi) = \mathbf{U}'_c(\xi)$, also called the *propagator mode*, is the corresponding eigenfunction. Because \mathcal{L} is in general not self-adjoint, the eigenfunction $\mathbf{W}^\dagger(\xi)$ of the adjoint operator \mathcal{L}^\dagger to eigenvalue zero, the so-called *response function*, is not identical to $\mathbf{W}(\xi)$. Expanding Eq. (6) with $\mathbf{u}_0 = \mathbf{U}_c(\xi) + \varepsilon \tilde{\mathbf{u}}$ up to $\mathcal{O}(\varepsilon)$ yields the PDE $\partial_t \tilde{\mathbf{u}} = \mathcal{L} \tilde{\mathbf{u}} + \mathbf{v}(\xi + c_0 t) \cdot \nabla \mathbf{U}_c$. Its solution $\tilde{\mathbf{u}}$ can be expressed in terms of eigenfunctions \mathbf{w}_i of \mathcal{L} as $\tilde{\mathbf{u}} = \sum_i a_i(t) \mathbf{w}_i(\xi)$ with expansion coefficients $a_i \sim \int_{t_0}^t d\tilde{t} e^{\lambda_i(t-\tilde{t})} b(\tilde{t})$ and b a functional of $\mathbb{D}(\mathbf{v} \cdot \nabla) \mathbf{u}_0$ involving eigenfunctions of \mathcal{L}^\dagger ; for details see Supplemental Material in Ref. [34]. By multiple scale theory for small perturbations of the order ε [34, 38, 39], the following equation of motion (EOM) for the position $\phi(t)$ of the TW in the presence of a boundary-induced advection term can be obtained

$$\dot{\phi}(t) = c_0 - \frac{1}{K_c} \int_{-\infty}^{\infty} d\xi \mathbf{W}^\dagger(\xi)^T \mathbb{D} \frac{Q'(\xi + \phi(t))}{Q(\xi + \phi(t))} \mathbf{U}'_c(\xi), \quad (9)$$

with constant $K_c = \int_{-\infty}^{\infty} d\xi \mathbf{W}^\dagger(\xi)^T \mathbf{U}'_c(\xi)$ and initial condition $\phi(t_0) = \phi_0$. For monotonically decreasing front solutions, we define its position ϕ as the point of steepest slope, while for pulse solutions it is the point of maximum amplitude of an arbitrary component. The EOM (9) only takes into account the contribution of the perturbation $\mathbb{D}(\mathbf{v} \cdot \nabla) \mathbf{u}_0$ projected on the response function $\mathbf{W}^\dagger(\xi)^T$ affecting the TW's position. Such EOM must be seen as the first two terms of an asymptotic series [40].

Since the integrand in Eq. (9) does not explicitly depend on time, the mean time T_c the TW needs to travel one period L_x is given by

$$T_c = \int_0^{L_x} d\phi \frac{1}{c_0 - \Theta(\phi)}, \quad (10)$$

and thus the average propagation velocity c reads

$$c = \frac{L_x}{T_c} = L_x / \int_0^{L_x} d\phi \frac{1}{c_0 - \Theta(\phi)}, \quad (11)$$

with substitute $\Theta(\phi) = \int_{-\infty}^{\infty} d\xi \mathbf{W}^\dagger(\xi)^T \mathbb{D} \frac{Q'(\xi + \phi)}{Q(\xi + \phi)} \mathbf{U}'_c / K_c$.

III. NUMERICAL RESULTS

In the work at hand, we limit our consideration to a single component system, $\mathbf{u} = u$, with bistable reaction kinetics. The associated RD system reads

$$\partial_t u = D_u \Delta u - u(u-a)(u-1), \quad 0 < a < 1 \quad (12)$$

in dimensionless form. The parameter a is related to the local excitation threshold of the medium while the rest state and the excited state are given by $u_{\text{rest}} = 0$ and $u_{\text{exc}} = 1$, respectively. This model was introduced by Zeldovich and Frank-Kamenetskii in the modeling of flame propagation in 1938 [41] and then applied by Schlögl to the description of a first-order non-equilibrium phase transition [42]. Traveling front solutions to Eq. (12) obey the Dirichlet boundary conditions $\lim_{x \rightarrow -\infty} u(\mathbf{r}, t) = u_{\text{exc}}$ and $\lim_{x \rightarrow \infty} u(\mathbf{r}, t) = u_{\text{rest}}$, respectively, and fulfills the condition $\lim_{\xi \rightarrow \pm\infty} \partial_\xi^n u = 0, \forall n \geq 1$.

In media with non-modulated cross-section $Q(x) = \text{const}$, Eq. (12) possesses a stable traveling front solution whose profile

$$u(\mathbf{r}, t) = U_c(\xi) = \frac{1}{1 + e^{\xi/\sqrt{2D_u}}}. \quad (13)$$

and the corresponding propagation velocity

$$c_0 = \sqrt{\frac{D_u}{2}} (1 - 2a), \quad (14)$$

are known analytically. The width of the traveling front defines the intrinsic length scale of the wave. Usually, for the Schlögl model the front width is defined as [42]

$$l_{\text{TW}} = \sqrt{32 D_u}. \quad (15)$$

Noteworthy, the front velocity depends on the excitation threshold a while the front profile and, consequently, the front width are independent of a . This is a peculiarity of the Schlögl model. We emphasize that the front width l_{TW} depends solely on the diffusion constant D_u in our scaling. Therefore, we can adjust the front width by means of the diffusion coefficient in the simulations. Furthermore, one can prove that the response function $W^\dagger(\xi)$ reads

$$W^\dagger(\xi) = e^{c_0 \xi / D_u} U'_c(\xi), \quad (16)$$

and thus the constant K_c is given by

$$K_c = \int_{-\infty}^{\infty} d\xi W^\dagger U'_c = \frac{\pi}{6} \frac{a(1-a)(1-2a)}{\sqrt{2D_u} \sin((1-2a)\pi)}. \quad (17)$$

For the profiles of the perpendicular side-walls we chose a sinusoidally modulated boundary function

$$\omega_+(x) = \begin{cases} 1 & , \text{for } x < 0, \\ \frac{1}{2} \left[1 + \delta + (1 - \delta) \cos\left(\frac{2\pi x}{L_x}\right) \right] & , \text{for } x \geq 0, \end{cases} \quad (18)$$

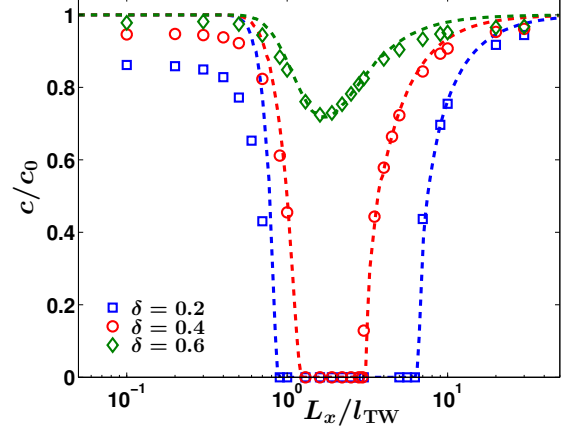


Figure 2. (Color online) Average front velocity c in units of the free velocity c_0 as a function of the ratio of period length L_x to front width l_{TW} for a sinusoidally modulated channel; see Fig. 1. The projection method (lines), Eq. (11), yields excellent agreement with the numerical results (markers); particularly, it reproduces the interval of propagation failure $c = 0$ for intermediate values of L_x/l_{TW} but fails for small ratios $L_x/l_{\text{TW}} \ll 1$. The remaining parameter values are set to $L_x = 5$ and $a = 0.4$.

for the upper wall and set the lower boundary to $\omega_-(x) = 0$. This setup is equivalent to study a reflection symmetric channel with twice the width, $\omega_\pm(x) = \pm\omega(x)$.

In what follows, we compare our analytic estimate for the average front velocity c , Eq. (11), with numerical results. Therefore, Eq. (12) supplemented with the Neumann b.c. Eq. (2) is solved numerically using finite element method (FEM) [43]. In our simulations, the front is initialized with $U_c(x - x_{\text{start}})$ at $x_{\text{start}} = \min(-4l_{\text{TW}}, -L_x)$ and simulated until it reaches $x_{\text{end}} = \max(10L_x, \text{ceil}(10l_{\text{TW}}/L_x)L_x)$. The data for the average front velocity c are determined from a linear fit to a position vs. time plot after subtracting transients.

In Fig. 2, we depict the average front velocity c in units of c_0 as a function of the ratio of period length L_x to front width l_{TW} . One observes a nonlinear dependence of c on the ratio L_x/l_{TW} : If the spatial period is much larger than the intrinsic width of the TW, $L_x \gg l_{\text{TW}}$, the front velocity equals c_0 . In this limit, the wave is well approximated by an isoconcentration line and one can assume that its velocity instantaneously adapts when transiting through the corrugated channel. Then, the average front velocity is correctly predicted by the harmonic mean velocity [33]

$$c_{\text{harm}} = L_x \int_0^{L_x} \frac{dx}{c_0 + D_u Q'(x)/Q(x)}, \quad (19)$$

which tends to c_0 for $L_x/l_{\text{TW}} \rightarrow \infty$. With decreasing ratio L_x/l_{TW} , i.e., either increasing the diffusion constant D_u or decreasing the period length L_x (presented in Fig. 3), the average propagation velocity lessens until

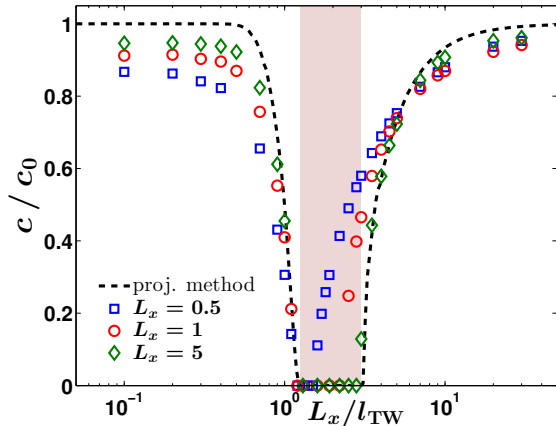


Figure 3. (Color online) Numerical results for propagation velocity c versus L_x/l_{TW} for various period lengths $L_x = 0.5$ (squares), $L_x = 1$ (circles), and $L_x = 5$ (diamonds). The corresponding values for the expansion parameter ε are $\varepsilon = 1.2, 0.6$, and $\varepsilon = 0.12$. The analytical prediction based on Eq. (11) is represented by the dashed line and the predicted interval of propagation failure is indicated by the light red block. The remaining parameter values are set to $a = 0.4$ and $\delta = 0.4$.

it attains its minimum value. Increasing the front width further, $L_x \lesssim l_{\text{TW}}$, the value of c grows and finally saturates at a value smaller than c_0 .

It turns out that both the minimum value of c and the saturation value depend crucially on the channel geometry; to be more precise on the bottleneck width δ . In general, we find that average front velocity diminishes with shrinking bottleneck width δ for a given ratio L_x/l_{TW} . In particular, we identify a finite interval of L_x/l_{TW} values where *propagation failure* occurs, i.e., the initially traveling front becomes quenched [44] and c goes to zero. One observes that the lower critical value of L_x/l_{TW} , where the propagation failure interval begins, shrinks with decreasing bottleneck width δ while the upper critical value, where the propagation failure interval ends, becomes larger for smaller bottlenecks. Consequently, the width of the propagation failure interval grows with decreasing value of δ . Lowering the excitation threshold while keeping the channel parameter L_x and δ constant facilitates the traveling front to transit through the corrugated media and thus the propagation failure interval disappears for $a \rightarrow 0$ (not shown explicitly).

Additionally, we compare our numerical results (markers) with the analytical prediction (lines), Eq. (11), in Fig. 2. Noteworthy, the projection method matches excellent with the numerics for all bottleneck widths δ ; particularly, it reproduces the finite interval of propagation failure for intermediate values of L_x/l_{TW} but it fails for small ratios $L_x/l_{\text{TW}} \ll 1$.

In Fig. 3, we illustrate a peculiarity of the projection method. The EOM for a traveling wave under the

boundary-induced perturbation Eq. (9) is determined by the convolution integral $\Theta(\phi)$ with kernel $W^\dagger(\xi)U'_c(\xi) = e^{c_0\xi}U'_c(\xi)^2$. The latter consists of the response function $W^\dagger(\xi)$ and the Goldstone mode U'_c both being localized around $\xi = 0$ and decay exponentially to zero if $|\xi| > l_{\text{TW}}$ for traveling fronts. On the other hand, the advection field $\mathbf{v}(x)$ changes periodically with period L_x . Therefore, the dynamics of the front position $\phi(t)$ and, consequently, the analytic result for the average front velocity c depend solely on the ratio of L_x to l_{TW} for a given set of δ and a values. This fact is shown in Fig. 3 where we present the propagation velocity c/c_0 for various period lengths, viz., $L_x = 0.5$ (squares), $L_x = 1$ (circles), and $L_x = 5$ (diamonds). The value of D_u is adjusted accordingly. It turns out that the analytic prediction based on project method Eq. (11) agrees well with the numerics for $L_x = 5$. With decreasing period length the range of applicability diminishes. This is in compliance with the assumptions made to derive Eq. (11): Both the asymptotic perturbation analysis, Sec. II A, and the multiple scale analysis, Sec. II B, require that the channel's cross-section changing rate $\max(|Q'(x)|) \propto \varepsilon$ is small. According to Eq. (3), the value of ε is inversely proportional to the period length L_x and thus the analytical prediction fails e.g. for $L_x = 0.5$ ($\varepsilon = 1.2$).

Moreover, we observe that the range of L_x/l_{TW} values where propagation failure occurs lessens with decreasing period length L_x . Remarkably, the lower critical value of L_x/l_{TW} seems to be independent of L_x .

A. Propagation failure – eikonal approach

Next, we present a quantitative explanation for the appearance of propagation failure for $L_x \gg l_{\text{TW}}$. If the intrinsic front width is much shorter than the spatial period, any front propagating through the channel geometry can be well approximated by one time-dependent curve $\gamma(s, t)$ tracing out a chosen isoconcentration line parametrized by s . A plane front $\gamma = (c_0 t, y)^T$ has constant velocity at all points in the forward, normal direction. If the plane geometry of the wave is distorted, here, due to the requirement that the edge of the wave front must propagate so that the TW always meets the boundary orthogonally, the normal velocity varies locally across the front.

When a front attempts to turn around a curved boundary, the entire front becomes curved and is well described by a circular arc with radius r_c touching orthogonally the boundary $\omega_+(x)$. The associated curvature at x^* is given by

$$\kappa(x^*) = \frac{1}{r_c} = \frac{1}{\omega_+(x^*)} \frac{\omega'_+(x^*)}{\sqrt{1 + \omega'_+(x^*)^2}} \simeq \frac{\omega'_+(x^*)}{\omega_+(x^*)}. \quad (20)$$

Comparing Eq. (9) and Eq. (20), one notices that the EOM for TWs resembles the linear eikonal equation [45,

46]

$$\dot{\phi}(t) \simeq c_0 - D_u \kappa(\phi), \quad (21)$$

in the limit $l_{\text{TW}} \ll L_x$, respectively, $W^\dagger(\xi)U'_c(\xi) \rightarrow \delta(\xi)$. According to Eq. (21), standing fronts exist and thus propagation failure occurs if the local curvature is equal to $\kappa(\phi) = c_0/D_u$. Grindrod et. al [47] demonstrated that stationary circular TW solutions are stable against deformations if the stability condition

$$\omega''_+(x*) \notin \left[0, \omega'_+(x*)^2 / (\omega_+(x*)(1 + \omega'_+(x*)^2)^2)\right] \quad (22)$$

holds at any $x* \in [0, L_x]$.

In order to determine the upper limit of L_x/l_{TW} , where the interval of propagation failure ends, first one has to find the roots of $0 = c_0 - D_u \kappa(x*)$ and secondly has to check if the stability condition Eq. (22) is not satisfied at $x*$. The dependence of the upper limit $(L_x/l_{\text{TW}})_{\text{up}}$ on the bottleneck width δ is depicted in Fig. 4. Moreover, we compare the analytic predictions based on the eikonal approach (lines) with the numerically obtained values for $(L_x/l_{\text{TW}})_{\text{up}}$ using FEM simulations (markers). Obviously, the agreement is excellent for small bottlenecks but fails for large values of δ . In channels with wide openings $\delta \rightarrow 1$ traveling waves have to curve only locally, close to edge of the wave front. Consequently, the isoconcentration lines $\gamma(s, t)$ are almost planar, i.e., the TW travels with almost constant velocity in x -direction, and propagation failure does not occur.

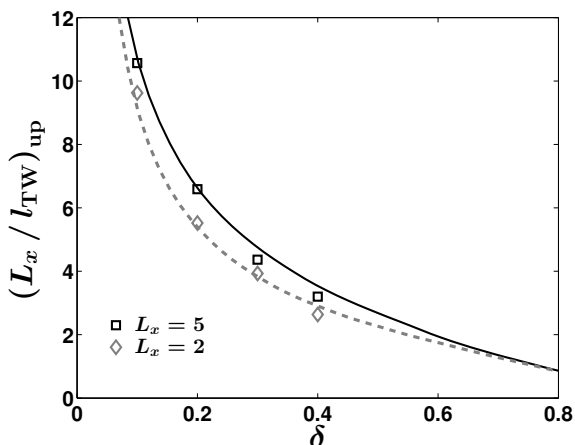


Figure 4. (Color online) Dependence of the upper limit $(L_x/l_{\text{TW}})_{\text{up}}$, where the interval of propagation failure ends, on the bottleneck width δ . The eikonal approach ($L_x = 2$: dashed line, $L_x = 5$: solid line), Eqs. (21)-(22), yields excellent agreement with the numerical results ($L_x = 2$: diamonds, $L_x = 5$: squares) for narrow channels $\delta \ll 1$ but fails for channels with wide openings. In simulations no propagation failure was found for $\delta \gtrsim 0.5$. The numerical errors are of the size of the markers.

IV. DIFFUSION LIMITED REGIME – CONFINED BROWNIAN MOTION

In the Figs. 2 and 3, we have shown that the average propagation velocity converges to a saturation value which is smaller than c_0 if the front width is much larger than the period of the channel geometry, $L_x/l_{\text{TW}} \rightarrow 0$. We emphasize that the projection method fails in this limit and predicts $c = c_0$ regardless of the value of L_x and δ . In contrast, the numerics show that the saturation value lessens with decreasing bottleneck width δ , cf. Fig. 2, and with shrinking period L_x , see Fig. 3; in a word, with growing value of $\varepsilon = (1 - \delta)/L_x$. If the intrinsic width $l_{\text{TW}} = \sqrt{32D_u}$ is much larger than the periodicity of the channel L_x , the front is extended over many periods and boundary interactions play a subordinate role. Then, the diffusion of reactants in longitudinal (x -) direction under spatially confined conditions is the predominant process for wave propagation and the full three-dimensional problem can be approximated by an effective one-dimensional description introducing an effective diffusion constant D_{eff}

$$\partial_t \mathbf{u}(\mathbf{r}, t) = D_{\text{eff}} \partial_x^2 \mathbf{u} + \mathbf{R}(\mathbf{u}). \quad (23)$$

Experimental [18, 19] and theoretical studies [21, 22] on particle transport in micro-domains with obstacles [48, 49] and/or small openings revealed that Brownian motion in such systems exhibits non-intuitive features like a significant suppression of particle diffusivity [20, 24, 50]. Numerous research activities in this topic led to the development of an approximate description of the diffusion problem – the *Fick-Jacobs approach* [51, 52]. The latter provides a powerful tool to describe particle transport through corrugated channel geometries and its accuracy has been intensively studied for diffusing particles in two- [23, 53] and three-dimensional channels [54–56]. The Fick-Jacobs approach predicts that the effective diffusion constant in longitudinal direction is solely determined by the variation of the cross-section $Q(x)$ and can be calculated according to the Lifson-Jackson formula [57]

$$D_{\text{eff}}^{\text{FJ}} = \frac{D_u}{\langle Q(x) \rangle_x \langle 1/Q(x) \rangle_x} \quad (24)$$

with period average $\langle \cdot \rangle_x = L_x^{-1} \int_0^{L_x} \cdot dx$. For the exemplarily considered channel geometry, Eq. (18), the value of D_{eff} is given by

$$D_{\text{eff}}^{\text{FJ}} = D_u \frac{2\sqrt{\delta}}{1 + \delta}. \quad (25)$$

Similar to the derivation of the reaction-diffusion-advection equation for \mathbf{u}_0 , see Sec. II A, the Fick-Jacobs approach is valid solely for weakly modulated channel geometries, i.e., $\max|Q'(x)| \propto \varepsilon \ll 1$. For moderate to strong corrugated boundaries correction terms have to be

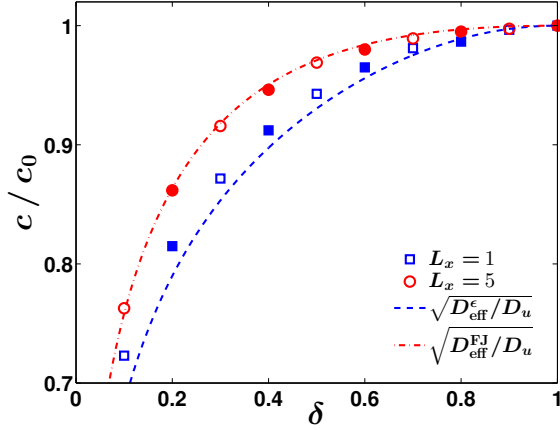


Figure 5. (Color online) Average front velocity c versus bottleneck width δ for different values of $a = 0.2$ (blank markers) and $a = 0.4$ (filled markers). The ratio L_x/l_{TW} is set to $L_x/l_{\text{TW}} = 0.1$ and the diffusion coefficient D_u is adjusted accordingly, viz., $D_u = 3.125$ ($L_x = 1$) and $D_u = 78.125$ ($L_x = 5$).

considered [31], yielding

$$D_{\text{eff}}^\varepsilon = D_u \frac{2 L_x \sqrt{\delta}}{\pi (1 - \delta^2)} \sinh(\pi (1 - \delta) / L_x). \quad (26)$$

For the studied Schlögl model, the average propagation velocity in units of the free velocity might be approximated well by $c/c_0 \simeq \sqrt{D_{\text{eff}}^{\text{FJ},\varepsilon}/D_u}$, cf. Eq. (14).

In Fig. 5, we present the impact of the bottleneck width δ on the propagation velocity c in units of c_0 for two different period lengths, viz., $L_x = 1$ and $L_x = 5$. In the numerics, the ratio L_x/l_{TW} is set to $L_x/l_{\text{TW}} = 0.1$ and the diffusion coefficient D_u is adjusted accordingly. One notices that the analytic estimate using $D_{\text{eff}}^{\text{FJ}}$, Eq. (25), agrees excellently with our simulation results for long period lengths $L_x = 5$ (circles) and small values of ε , $\varepsilon \in [0, 0.2]$, respectively. For smaller periods, $L_x = 1$ (squares), higher order corrections to the effective diffusion coefficient Eq. (26) are necessary in order to ensure a good agreement between numerics and analytics. The corresponding value for the expansion parameter ε , Eq. (3), ranges from zero to unity. Remarkably, the saturation value for the front velocity in units of its free value c_0 is independent of the value for the excitation threshold a and thus solely determined by the spatial variations of the channel cross-section $Q(x)$; to sum up, $c \simeq \sqrt{0.5 D_{\text{eff}}(Q(x))(1 - 2a)}$ for $l_{\text{TW}} \gg L_x$.

Interestingly, the propagation of traveling fronts through 3D channels with spatially modulated cross-sections can be well treated by a one-dimensional RD equation Eq. (23). Within the latter, the impact of the spatial variations on the reactants' microscopic dynamics is neglected. This enables us to treat the problem macroscopically. However, the influence of boundary modulation on diffusive transport of material is hidden in an

artificially introduced effective diffusion coefficient D_{eff} . To estimate the value of D_{eff} detailed information about the local cross-section is needed.

V. CONCLUSION

We address the problem of traveling wave propagation through a 3D reaction medium with periodically modulated cross-section. Supposing that the channel's cross-section changes weakly, we apply asymptotic perturbation analysis in the geometric parameter ε to the problem. This leads to an approximate description that involves a reduction of dimensionality, from 3D to 1D. The Neumann boundary conditions on reactants in the original system translate into an additional *boundary-induced advection term*. The latter is proportional to the spatial variation of the cross-section and hence one can interpret the advection term as a weak spatio-temporal perturbation to a one-dimensional reaction-diffusion system. Utilizing the powerful projection method, also known as multiple scale perturbation theory, we obtain an equation of motion for the traveling wave position in the presence of the boundary-induced advection term. Furthermore, analytical expressions for the average propagation velocity of traveling waves c in corrugated channels are derived. The comparison between the analytical and the numerical results demonstrate that the analytical methods properly predicts the dependence of the propagation velocity on the spatial period of the channel geometry L_x , the intrinsic width of the wave pattern l_{TW} , and the bottleneck width δ ; including the peculiarity of *propagation failure*.

Exemplary, we study the impact of a sinusoidally modulated cross-section on the propagation of traveling front solutions in a one-component Schlögl model. It turns out that the propagation velocity exhibits a nonlinear dependence on the ratio of the spatial period L_x to the intrinsic width of the front l_{TW} :

If the period is much larger than the intrinsic width, $L_x \gg l_{\text{TW}}$, the average front velocity is correctly predicted by the harmonic mean velocity which tends to the velocity value for non-modulated media c_0 . With decreasing ratio L_x/l_{TW} the average propagation velocity lessens until it attains its minimum value. Reducing the ratio further, $L_x \lesssim l_{\text{TW}}$, the front velocity starts to grow again and finally saturate at a value smaller than c_0 .

For intermediate values of L_x/l_{TW} , the minimum value of c diminishes with shrinking bottleneck width. In particular, we identify a finite interval of L_x/l_{TW} values where *propagation failure* occurs, i.e., the initially traveling front becomes quenched inside the corrugated channel and hence the average propagation velocity goes to zero. We observe that the lower critical value of L_x/l_{TW} , where the propagation failure interval begins, shrinks with decreasing bottleneck width and it is independent of the spatial period L_x . On the other hand, the upper critical value, where the propagation failure interval ends, be-

comes larger for smaller bottlenecks and longer periods L_x . The existence of propagation failure and, in particular, the dependence of the upper critical value of L_x/l_{TW} can be predicted excellently by the eikonal approach.

If the period is small, $L_x/l_{\text{TW}} \ll 1$, the front velocity saturates at an asymptotic value which is determined solely by the shape of the cross-section. In this limit, the traveling front dynamics is dominated by the diffusive motion of the reactants under spatially confined conditions. We demonstrate that the Neumann boundary conditions on the reactants in the complete 3D system translate into a one-dimensional reaction-diffusion system with an effective diffusion coefficient (effective medium theory). Thereby, the influence of the boundary modulation on the microscopic dynamics is hidden in the value of D_{eff} . Noteworthy, we present analytical estimates for the value of D_{eff} which agree excellently with our simulation results.

Regarding the applicability of the asymptotic pertur-

bation analysis and the projection method to our problem, it is quite remarkable that both approaches lead to a very good agreement with the numerical simulations for a large range of spatial periods and bottleneck widths. Both methods require that the channel's cross-section changing rate $\max(|Q'(x)|) \propto \varepsilon$ is small. Consequently, discrepancies occur for geometries with small spatial periods and narrow openings.

ACKNOWLEDGMENTS

We acknowledge support by the DFG through SFB 910 (S. M and H. E.) and GRK 1558 (J. L.).

ACKNOWLEDGMENTS

We acknowledge support by the DFG through SFB 910 (S. M and H. E.) and GRK 1558 (J. L.).

-
- [1] M. Cross and P. Hohenberg, Rev. Mod. Phys. **65**, 851 (1993).
 - [2] J. Murray, *Mathematical Biology* (Springer-Verlag, Berlin, 2003).
 - [3] P. C. Bressloff and J. M. Newby, Rev. Mod. Phys. **85**, 135 (2013).
 - [4] E. Newman and K. Zahs, Science **275**, 844 (1997).
 - [5] Y. Kuramoto, *Chemical Oscillations, Waves, and Turbulence* (Courier Dover Publications, New York, 2003).
 - [6] R. Kapral and K. Showalter, eds., *Chemical Waves and Patterns* (Kluwer, Dordrecht, 1995).
 - [7] M. Bär, C. Zülicke, M. Eiswirth, and G. Ertl, J. Phys. Chem. **96**, 8595 (1992); M. Bär, I. G. Kevrekidis, H. H. Rotermund, and G. Ertl, Phys. Rev. E **52**, R5739 (1995).
 - [8] J. P. Voroney, A. T. Lawniczak, and R. Kapral, Physica D **99**, 303 (1996).
 - [9] S. Y. Shvartsman, E. Schütz, R. Imbühl, and I. G. Kevrekidis, Phys. Rev. Lett. **83**, 2857 (1999).
 - [10] H. H. Rotermund, Surface Science **603**, 1662 (2009).
 - [11] J. Laplante and T. Erneux, J. Phys. Chem. **96**, 4931 (1992).
 - [12] F. Haudin, R. G. Elias, R. G. Rojas, U. Bortolozzo, M. G. Clerc, and S. Residori, Phys. Rev. Lett. **103**, 128003 (2009).
 - [13] H. R. Petty, .
 - [14] S. Atis, S. Saha, H. Auradou, D. Salin, and L. Talon, Phys. Rev. Lett. **110**, 148301 (2013).
 - [15] E. Beerdse, D. Dubbeldam, and B. Smit, Phys. Rev. Lett. **96**, 044501 (2006).
 - [16] L. D. Gelb, K. E. Gubbins, R. Radhakrishnan, and M. Sliwinka-Bartkowiak, Rep. Prog. Phys. **62**, 1573 (1999).
 - [17] I. Santamaria-Holek, Z. J. Grzywna, and J. M. Rubí, Eur. Phys. J. - Spec. Top. **222**, 129?141 (2013).
 - [18] A. S. Verkman, Trends Biochem. **27**, 27 (2002).
 - [19] A. Corma, Chem. Rev. **97**, 2373 (1997).
 - [20] S. L. Dettmer, S. Pagliara, K. Misiunas, and U. F. Keyser, Rev. Sci. Instrum. **85** (2014), 10.1063/1.4865552; ArXiv e-prints (2014), arXiv:1402.7037.
 - [21] D. Reguera, G. Schmid, P. S. Burada, J. M. Rubí, P. Reimann, and P. Hänggi, Phys. Rev. Lett. **96**, 130603 (2006).
 - [22] P. S. Burada, G. Schmid, P. Talkner, P. Hänggi, D. Reguera, and J. M. Rubí, BioSystems **93**, 16 (2008).
 - [23] P. Burada, P. Hänggi, F. Marchesoni, G. Schmid, and P. Talkner, ChemPhysChem **10**, 45 (2009).
 - [24] S. Martens, A. V. Straube, G. Schmid, L. Schimansky-Geier, and P. Hänggi, Phys. Rev. Lett. **110**, 010601 (2013).
 - [25] G. Haas, M. Bär, I. G. Kevrekidis, P. B. Rasmussen, H. H. Rotermund, and G. Ertl, Phys. Rev. Lett. **75**, 3560 (1995).
 - [26] B. F. Edwards, Phys. Rev. Lett. **89**, 104501 (2002).
 - [27] D. A. Vasquez, Phys. Rev. Lett. **93**, 104501 (2004).
 - [28] E. Cherry and F. Fenton, J. Theo. Biol. **285**, 164 (2011).
 - [29] A. Azhand, J. F. Totz, and H. Engel, ArXiv e-prints (2014), arXiv:1406.5964.
 - [30] J. F. Totz, H. Engel, and O. Steinbock, ArXiv e-prints (2014), arXiv:1401.6550.
 - [31] S. Martens, G. Schmid, L. Schimansky-Geier, and P. Hänggi, Phys. Rev. E **83**, 051135 (2011); Chaos **21**, 047518 (2011).
 - [32] L. Schimansky-Geier, A. S. Mikhailov, and W. Ebeling, Annalen der Physik **495**, 277 (1983); A. Engel, Phys. Lett. A **113**, 139 (1985).
 - [33] J. Löber, M. Bär, and H. Engel, Phys. Rev. E **86**, 066210 (2012).
 - [34] J. Löber and H. Engel, Phys. Rev. Lett. **112**, 148305 (2014).
 - [35] J. X. Xin, SIAM Rev. **42**, 161 (2000).
 - [36] P. S. Burada, G. Schmid, and P. Hänggi, Phil. Trans. R. Soc. A **367**, 3157 (2009).

- [37] S. Martens, I. M. Sokolov, and L. Schimansky-Geier, J. Chem. Phys. **136**, 111102 (2012).
- [38] H.-G. Purwins, H.-U. Bödeker, and A. W. Liehr, *Dissipative solitons in reaction-diffusion systems* (Springer, 2005) pp. 267–308.
- [39] J. Löber, Phys. Rev. E **89**, 062904 (2014).
- [40] C. M. Bender and S. A. Orszag, *Advanced Mathematical Methods for Scientists and Engineers* (McGraw-Hill, New York, 1978).
- [41] Y. Zeldovich and D. Frank-Kamenetsky, Dokl. Akad. Nauk SSSR **19**, 693 (1938).
- [42] F. Schlögl, Z. Phys.A **253**, 147 (1972).
- [43] F. Hecht, J. Numer. Math. **20**, 251 (2012); O. Pironneau, F. Hecht, and J. Morice, “FreeFEM++,” (2012).
- [44] J. X. Xin and J. Zhu, Physica D **81**, 94 (1995).
- [45] J. Keener, SIAM J. Appl. Math. **46**, 1039 (1986).
- [46] H. Dierckx, O. Bernus, and H. Verschelde, Phys. Rev. Lett. **107**, 108101 (2011).
- [47] P. Grindrod, M. A. Lewis, and J. D. Murray, Proc. R. Soc. Lond. A **433**, 151 (1991).
- [48] L. Dagdug, M.-V. Vazquez, A. M. Berezhkovskii, V. Y. Zitserman, and S. M. Bezrukov, J. Chem. Phys. **136**, 204106 (2012).
- [49] P. K. Ghosh, P. Hänggi, F. Marchesoni, S. Martens, F. Nori, L. Schimansky-Geier, and G. Schmid, Phys. Rev. E **85**, 011101 (2012).
- [50] A. E. Cohen and W. E. Moerner, Proc. Nat. Ac. Sc. U.S.A **103**, 4362 (2006).
- [51] M. Jacobs, *Diffusion Processes*, 2nd ed. (Springer, New York, 1967).
- [52] R. Zwanzig, J. Phys. Chem. **96**, 3926 (1992).
- [53] D. Reguera and J. M. Rubí, Phys. Rev. E **64**, 061106 (2001).
- [54] B.-q. Ai and L.-g. Liu, Phys. Rev. E **74**, 051114 (2006).
- [55] L. Dagdug, A. M. Berezhkovskii, Y. A. Makhnovskii, V. Y. Zitserman, and S. M. Bezrukov, J. Chem. Phys. **134**, 101102 (2011).
- [56] A. M. Berezhkovskii, M. A. Pustovoi, and S. M. Bezrukov, J. Chem. Phys. **126**, 134706 (2007).
- [57] S. Lifson and J. L. Jackson, J. Chem. Phys. **36**, 2410 (1962).